Advances in Applied Mathematics and Mechanics
Adv. Appl. Math. Mech., Vol. **3**, No. 4, pp. 470-492

DOI: 10.4208/aamm.10-m1056
August 2011

Mathematical Development and Verification of a Finite Volume Model for Morphodynamic Flow Applications

Fayssal Benkhaldoun[1,*], Mohammed Seaïd[2] and Slah Sahmim[3]

[1] *LAGA, Université Paris* 13, 99 *Av J.B. Clement*, 93430 *Villetaneuse, France*
[2] *School of Engineering and Computing Sciences, University of Durham, South Road, Durham DH1 3LE, UK*
[3] *Laboratoire D'ingénierie Mathématique, Ecole Polytechnique de Tunisie, B.P. 743-2078 La Marsa, Tunisia*

Received 23 September 2010; Accepted (in revised version) 23 December 2010

Available online 10 July 2011

Abstract. The accuracy and efficiency of a class of finite volume methods are investigated for numerical solution of morphodynamic problems in one space dimension. The governing equations consist of two components, namely a hydraulic part described by the shallow water equations and a sediment part described by the Exner equation. Based on different formulations of the morphodynamic equations, we propose a family of three finite volume methods. The numerical fluxes are reconstructed using a modified Roe's scheme that incorporates, in its reconstruction, the sign of the Jacobian matrix in the morphodynamic system. A well-balanced discretization is used for the treatment of the source terms. The method is well-balanced, non-oscillatory and suitable for both slow and rapid interactions between hydraulic flow and sediment transport. The obtained results for several morphodynamic problems are considered to be representative, and might be helpful for a fair rating of finite volume solution schemes, particularly in long time computations.

AMS subject classifications: 65M08, 76B15, 76M12

Key words: Morphodynamic model, shallow water equations, sediment transport, finite volume method, well-balanced discretization.

1 Introduction

The main concern of morphodynamics is to determine the evolution of bed levels for hydrodynamic systems such as rivers, estuaries, bays and other nearshore regions

*Corresponding author.
URL: `http://www.math.univ-paris13.fr/~fayssal/`
Email: fayssal@math.univ-paris13.fr (F. Benkhaldoun), m.seaid@durham.ac.uk (M. Seaïd), s.sahmim@gmail.com (S. Sahmim)

where water flows interact with the bed geometry. Example of applications include among others, beach profile changes due to severe wave climates, seabed response to dredging procedures or imposed structures, and harbour siltation. The ability to design numerical methods able to predict the morphodynamic evolution of the coastal seabed has a clear mathematical and engineering relevances. In practice, morphodynamic problems involve coupling between a hydrodynamic model, which provides a description of the flow field leading to a specification of local sediment transport rates, and an equation for bed level change which expresses the conservative balance of sediment volume and its continual redistribution with time. In the current study, the hydrodynamic model is described by the shallow water equations and the sediment transport is modelled by the Exner equation. The coupled models form a hyperbolic system of conservation laws with a source term.

Nowadays, much effort has been devoted to develop numerical schemes for morphodynamic models able to resolve all hydrodynamic and morphodynamic scales. Special attention has been given to the treatment of the source term and the bedload flux. It is well known that shallow water equations on nonflat topography have steady-state solutions in which the flux gradients are nonzero but exactly balanced by the source terms. This well-balanced concept is also known by conservation property (C-property), compare [4, 20] among others. The well-established Roe's scheme [16] has been modified in [9] for the sediment transport problems. However, for practical applications, this method may become computationally demanding due to its treatment of the source terms. Numerical methods based on Euler-WENO techniques have also been applied to sediment transport equations in [13]. Authors in [6] extended the ENO and WENO schemes to sediment transport equations, whereas the CWENO method has been applied to sediment transport problems in [5]. Unfortunately, most ENO, WENO and CWENO methods that solves real morphodynamic models correctly are still very computationally expensive. On the other hand, numerical methods using the relaxation approximation have also been applied to sediment transport equations in [8]. The relaxation schemes employ general higher order reconstruction for spatial discretization and higher order implicit-explicit schemes or TVD Runge-Kutta schemes for time integration of the relaxing systems. It is well known that TVD schemes have their order of accuracy reduced to first order in the presence of shocks due to the effects of limiters.

The object of this study is to devise a numerical approach able to accurately approximate solution to morphodynamic problems. Our aim is to develop a family of finite volume methods based on a non-homogeneous Riemann solver for solving morphodynamic models. The methods have been investigated in [18, 19] for numerical solution of conservation laws with source terms and are adapted in the current work for the numerical solution of morphodynamic problems. The proposed finite volume scheme belongs to the class of methods that employ only physical fluxes and averaged states in their formulations. To control the local diffusion in the scheme and also to preserve monotonicity, a parameter is introduced based on the sign matrix of the flux Jacobian. The main characteristics of such a finite volume scheme are on

one hand, the capability to satisfy the C-property resulting in numerical solutions free from spurious oscillations in significant morphodynamic situations, and on the other hand the achievement of strong stability for simulations of slowly varying bed-load as well as rapidly varying flows containing also shocks or discontinuities. These characteristics are verified using three test examples of the evolution of an initial bed with different shapes in a channel. Results presented in this paper show high resolution of the proposed finite volume schemes and permit the straightforward application of the method to more complex, physically based morphodynamic models.

Recently, the authors in [2,3] have presented numerical results for two-dimensional sediment transport problems using only one formulation of the equations. In the current study we present numerical results obtained using different formulations of the equations governing the morphodynamic problems. Some results are presented as validation examples and others, to the best of our knowledge, are reported for the first time. In this paper, first the governing equations for the morphodynamic problems are formulated. Thereafter, a well-balanced finite volume method employed to solve the morphodynamic problems is presented for different formulations. After experiments with the different approaches for a variety of morphodynamic examples, accuracy and efficiency of the finite volume schemes are discussed. Concluding remarks end the paper.

2 Governing equations for the morphodynamic problems

In practical morphodynamic applications, the hydraulic flow is usually modelled by the shallow water equations. These equations consist of the conservation of mass and momentum balance

$$\partial_t h + \partial_x(hu) = 0, \tag{2.1a}$$

$$\partial_t(hu) + \partial_x\Big(hu^2 + \frac{1}{2}gh^2\Big) = -gh\partial_x B, \tag{2.1b}$$

where h is the water height above the bottom, u is the water velocity, g is the acceleration due to gravity, and B is the function characterizing the bed level. For fixed bottom topography, i.e., $B = B(x)$, the Eq. (2.1) reduce to the standard shallow water equations. In the current work, we assume that a sediment transport takes place such that the bed level depends on time variable as well. This requires an additional equation for its evolution. Here, the equation used to update the bed-load is given by the well-known Exner equation

$$(1-p)\partial_t B + \partial_x q = 0, \tag{2.2}$$

where p is the porosity assumed to be constant and q is the sediment transport flux and it depends on the type of sediment. As an example, we consider the basic sediment transport flux [10]

$$q(u) = Au|u|^{m-1}, \tag{2.3}$$

where A is a given experimental constant and $1 \leq m \leq 4$ is a chosen parameter. Note that the Eq. (2.2) states that the time rate of change of the bed elevation is equal to the divergence of the sediment flux, which can be expressed in terms of the local flow properties through the use of the empirical sediment formula (2.3). The typical value $m = 3$ is widely used in the literature, see for example [3,5,6,8,9], and it is used in all simulations presented in this paper. For simplicity in presentation, the Eqs. (2.1) and (2.2) can be rearranged in a system of conservation laws with a source term as

$$\partial_t \mathbf{W} + \partial_x \mathbf{F}(\mathbf{W}) = \mathbf{Q}(\mathbf{W}), \tag{2.4}$$

where

$$\mathbf{W} = \begin{pmatrix} h \\ hu \\ B \end{pmatrix}, \quad \mathbf{F}(\mathbf{W}) = \begin{pmatrix} hu \\ hu^2 + \frac{1}{2}gh^2 \\ \frac{1}{1-p}q \end{pmatrix}, \quad \mathbf{Q}(\mathbf{W}) = \begin{pmatrix} 0 \\ -gh\partial_x B \\ 0 \end{pmatrix}.$$

It is clear that the system (2.4) is hyperbolic and the associated eigenvalues λ_k ($k = 1,2,3$) are the zeros of the characteristic polynomial

$$P(\lambda) = -\lambda(\lambda^2 - 2u\lambda + u^2 - gh).$$

The eigenvalues of the Jacobian matrix are

$$\lambda_1 = u - \sqrt{gh}, \quad \lambda_2 = 0 \quad \text{and} \qquad \lambda_3 = u + \sqrt{gh}. \tag{2.5}$$

Observe that the Jacobian matrix in (2.4) is singular, which may causes severe numerical difficulties in many finite volume schemes, compare for example [9]. In fact, for a singular Jacobian matrix, the system becomes ill-conditioned and one cannot guarantee convergence in its numerical solution. For most hyperbolic systems of this type, a special treatment (known by entropy fix) is required for their finite volume solutions, see for instance [11] and further details are therein. In order to avoid this singularity, a modified system can be obtained by incorporating the bed into the flux function and the resulting system reads

$$\partial_t \widetilde{\mathbf{W}} + \partial_x \widetilde{\mathbf{F}}(\widetilde{\mathbf{W}}) = \widetilde{\mathbf{Q}}(\widetilde{\mathbf{W}}), \tag{2.6}$$

where

$$\widetilde{\mathbf{W}} = \begin{pmatrix} h \\ hu \\ B \end{pmatrix}, \quad \widetilde{\mathbf{F}}(\widetilde{\mathbf{W}}) = \begin{pmatrix} hu \\ hu^2 + \frac{1}{2}gh^2 + ghB \\ \frac{1}{1-p}q \end{pmatrix}, \quad \widetilde{\mathbf{Q}}(\widetilde{\mathbf{W}}) = \begin{pmatrix} 0 \\ gB\partial_x h \\ 0 \end{pmatrix}.$$

As mentioned in [6], using the Exner equation (2.2) to model the sediment transport, the nonhomegenuous terms in the right-hand side in (2.4) and (2.6) are not standard source terms but nonconservative products, since they include a derivative of one of

the variables. The presence of these terms in sediment transport system can cause sever difficulties in their numerical approximations. In principle, the nonhomegenuous term in these equations can be viewed as a source term and/or a nonconservative term. In [9] and in all approaches presented in this study these terms are considered and discretized as source terms.

Again, the system (2.6) is hyperbolic and the associated eigenvalues $\widetilde{\lambda}_k$ $(k=1,2,3)$ are the zeros of the characteristic polynomial

$$P(\widetilde{\lambda}) = \widetilde{\lambda}^3 - 2u\widetilde{\lambda}^2 + (u^2 - g(h+B+hd))\widetilde{\lambda} + ghud, \tag{2.7}$$

with

$$d = \frac{1}{(1-p)h} Am|u|^{m-1}.$$

The analytical expressions of the eigenvalues are

$$\widetilde{\lambda}_1 = 2\sqrt{-Q}\cos\Big(\frac{1}{3}\theta\Big) + \frac{2}{3}u, \tag{2.8a}$$

$$\widetilde{\lambda}_2 = 2\sqrt{-Q}\cos\Big[\frac{1}{3}(\theta+2\pi)\Big] + \frac{2}{3}u, \tag{2.8b}$$

$$\widetilde{\lambda}_3 = 2\sqrt{-Q}\cos\Big[\frac{1}{3}(\theta+4\pi)\Big] + \frac{2}{3}u, \tag{2.8c}$$

where

$$\theta = \arccos\Big(\frac{R}{\sqrt{-Q^3}}\Big),$$

with

$$Q = -\frac{1}{9}\big(u^2 + 3g(h+B+hd)\big), \qquad R = -\frac{u}{54}\big(-9g(2h+2B-hd) + 2u^2\big).$$

The Eqs. (2.1) and (2.2) can also be formulated using the physical variables as

$$\partial_t \mathbf{U} + \partial_x \mathbf{G}(\mathbf{U}) = \mathbf{0}, \tag{2.9}$$

where

$$\mathbf{U} = \begin{pmatrix} h \\ u \\ B \end{pmatrix}, \qquad \mathbf{G}(\mathbf{U}) = \begin{pmatrix} hu \\ \frac{1}{2}u^2 + g(h+B) \\ \frac{1}{1-p}q \end{pmatrix}.$$

The eigenvalues μ_k $(k=1,2,3)$ associated with the Jacobian matrix in (2.9) are the zeros of the characteristic polynomial

$$P(\mu) = \mu^3 - 2u\mu^2 + \big(u^2 - g(h+d)\big)\mu + gud, \tag{2.10}$$

with

$$d = \frac{1}{(1-p)} Am|u|^{m-1}.$$

Thus, the eigenvalues of the Jacobian matrix are

$$\mu_1 = 2\sqrt{-Q}\cos\Big(\frac{1}{3}\theta\Big) + \frac{2}{3}u, \tag{2.11a}$$

$$\mu_2 = 2\sqrt{-Q}\cos\Big[\frac{1}{3}(\theta+2\pi)\Big] + \frac{2}{3}u, \tag{2.11b}$$

$$\mu_3 = 2\sqrt{-Q}\cos\Big[\frac{1}{3}(\theta+4\pi)\Big] + \frac{2}{3}u, \tag{2.11c}$$

where

$$\theta = \arccos\Big(\frac{R}{\sqrt{-Q^3}}\Big),$$

with

$$Q = -\frac{1}{9}\big(u^2+3g(h+d)\big), \qquad R = \frac{u}{54}\big(9g(2h-d)-2u^2\big).$$

It should be stressed that the considered morphodynamical systems have to be solved in a spatial domain and for a time interval endowed with given initial and boundary conditions. In practice, these conditions are problem dependent and their discussion is postponed for Section 7 where numerical examples will be presented.

3 A class of finite volume methods

Let us discretize the spatial domain into control volumes $[x_{i-1/2}, x_{i+1/2}]$ with uniform size

$$\Delta x = x_{i+\frac{1}{2}} - x_{i-\frac{1}{2}},$$

and divide the temporal domain into subintervals $[t_n, t_{n+1}]$ with uniform size Δt. In order to explain the main ideas of the proposed finite volume method we consider the scalar equation of conservation law with a source term

$$\partial_t W + \partial_x F(W) = Q(W). \tag{3.1}$$

Following the standard finite volume formulation, we integrate the Eq. (3.1) with respect to time and space over the domain $[t_n, t_{n+1}] \times [x_{i-1/2}, x_{i+1/2}]$ to obtain the following discrete equation

$$W_i^{n+1} = W_i^n - \frac{\Delta t}{\Delta x}\big(F(W_{i+\frac{1}{2}}^n) - F(W_{i-\frac{1}{2}}^n)\big) + \Delta t Q_i^n, \tag{3.2}$$

where W_i^n is the space average of the solution W in the control volume $[x_{i-1/2}, x_{i+1/2}]$ at time t_n, i.e.,

$$W_i^n = \frac{1}{\Delta t \Delta x}\int_{t_n}^{t_{n+1}}\int_{x_{i-\frac{1}{2}}}^{x_{i+\frac{1}{2}}} W(t,x)\,dt\,dx,$$

and $F(W_{i\pm1/2}^n)$ are the numerical fluxes at $x = x_{i\pm1/2}$ and time t_n. The spatial discretization of the Eq. (3.2) is complete when a numerical construction of the fluxes $F(W_{i\pm1/2}^n)$ is chosen.

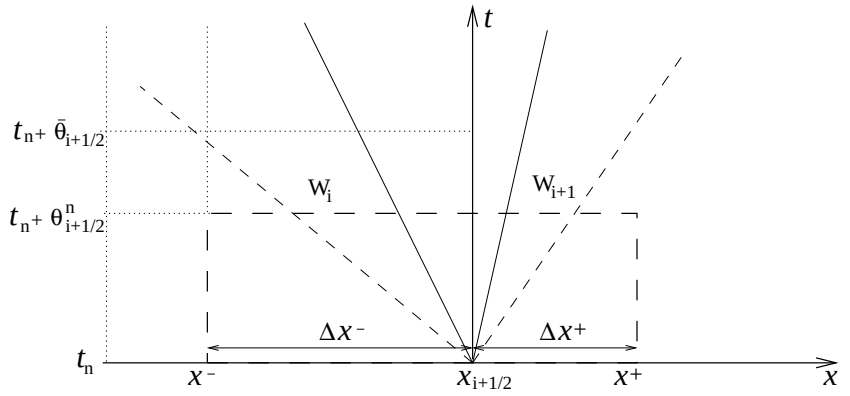

Figure 1: Modified Riemann problem in the proposed finite volume method.

In general, this construction requires a solution of Riemann problems at the interfaces $x_{i\pm1/2}$. From a computational viewpoint, this procedure is very demanding and may restricts the application of the method for which Riemann solutions are not available. Furthermore, since the source term in (3.2) is a nonconservative product, its discretization may suffer from singular values raised from the Riemann solution at the interfaces. For details, we refer the reader to the work of [20]. This difficulties are typical in numerical solution of shallow water equations on non-flat bottom rather than moving bed. In the current study we adapt a class of finite volume methods proposed in [18, 19] for numerical solution of conservation laws with source terms. The key idea is to reintegrate the Eq. (3.1) over a control domain $[t_n, t_n+\theta^n_{i+1/2}]\times[x^-, x^+]$ containing the point $(t_n, x_{i+1/2})$ as depicted in Fig. 1. It should be stressed that, the integration of the Eq. (3.1) over the control domain $[t_n, t_n+\theta^n_{i+1/2}]\times[x^-, x^+]$ is used only at a predictor stage to construct the intermediate states $W^n_{i\pm1/2}$ which will be used in the corrector stage (3.2). Here, $W^n_{i\pm1/2}$ can be interpreted as an approximation of the averaged Riemann solution R_s over the control volume $[x^-, x^+]$ at time $t_n+\theta^n_{i+1/2}$. Thus, the resulting intermediate state $W^n_{i+1/2}$ is given by

$$W^n_{i+\frac{1}{2}} = \frac{1}{2}\big(W^n_i + W^n_{i+1}\big) - \frac{1}{\Delta x}\theta^n_{i+\frac{1}{2}}\big(F(W^n_{i+1}) - F(W^n_i)\big) + \theta^n_{i+\frac{1}{2}}Q^n_{i+\frac{1}{2}}, \tag{3.3}$$

where W^n_i denotes the space average of the solution W at time t_n in the cell $[x^-, x^+]$ given by

$$W^n_i = \frac{1}{\Delta x^- + \Delta x^+}\int_{x^-}^{x^+} W(x, t_n)dx, \tag{3.4}$$

and $W^n_{i+1/2}$ is an approximate average of the solution W in the time-space domain $[t_n, t_n+\theta^n_{i+1/2}]\times[x_i, x_{i+1}]$ defined as

$$W^n_{i+\frac{1}{2}} = \frac{1}{\Delta x^- + \Delta x^+}\int_{x^-}^{x^+} W\big(x, t_n+\theta^n_{i+\frac{1}{2}}\big)dx. \tag{3.5}$$

In (3.3), $Q^n_{i+1/2}$ is an approximation of the averaged source term Q, i.e.,

$$Q^n_{i+\frac{1}{2}} = \frac{1}{\Delta t \Delta x} \int_{t_n}^{t_n+\theta^n_{i+\frac{1}{2}}} \int_{x^-}^{x^+} Q(W)\, dt\, dx.$$

The distance measures Δx^- and Δx^+ appeared in (3.4) and (3.5) are defined as

$$\Delta x^- = \left|x^- - x_{i+\frac{1}{2}}\right|, \qquad \Delta x^+ = \left|x^+ - x_{i+\frac{1}{2}}\right|.$$

Note that in order to complete the implementation of the above finite volume method, the parameters x^-, x^+, $\theta^n_{i+1/2}$ and $Q^n_{i+1/2}$ have to be selected. In the present study, a simple choice of the points

$$x^- = x_i \quad \text{and} \quad x^+ = x_{i+1},$$

is selected, but other selections are also possible. Based on the stability analysis reported in [19] for conservation laws with source terms, the variable $\theta^n_{j+1/2}$ is selected as

$$\theta^n_{i+\frac{1}{2}} = \alpha^n_{i+\frac{1}{2}} \bar{\theta}_{i+\frac{1}{2}}, \qquad \bar{\theta}_{i+\frac{1}{2}} = \Delta x \left(2S^n_{i+\frac{1}{2}}\right)^{-1}, \tag{3.6}$$

where

$$S^n_{i+\frac{1}{2}} = \max\left\{|F'(W^n_i)|, |F'(W^n_{i+1})|\right\},$$

is the local Rusanov's velocity and $\alpha^n_{i+1/2}$ is a positive parameter to be calculated locally. It is clear that, by setting

$$\alpha^n_{i+\frac{1}{2}} = 1,$$

the proposed finite volume method reduces to the well-known Rusanov method in the linear homogeneous case, whereas for

$$\alpha^n_{i+\frac{1}{2}} = \frac{\Delta t}{\Delta x},$$

one recovers the Lax-Wendroff scheme.

The application of the proposed finite volume method for systems of conservation laws with source terms has been investigated in [18, 19]. According to the analysis performed in the abovementioned references, the control parameter $\alpha^n_{j+1/2}$ has to be selected as a sign matrix of the Jacobian matrix of the system under consideration. It should be noted that the finite volume methods proposed in the present work can be interpreted as a predictor-corrector procedure. In the predictor stage, the averaged states $\mathbf{W}^n_{i+1/2}$ are computed whereas, the solution $\mathbf{W}^{n+1}_i$ is updated in the corrector stage. It is worth pointing out that, for homogeneous systems, i.e.,

$$\mathbf{Q} = 0,$$

the proposed finite volume method yields the VFRoe scheme studied in [14]. In what follows we discuss the formulation of the method for solving the morphodynamic system using different approaches.

3.1 Approach A

This approach uses the conservative variables in both the predictor and corrector stages. This results in the following scheme for the morphodynamic system (2.6):

$$\widetilde{\mathbf{W}}_{i+\frac{1}{2}}^{n}=\frac{1}{2}\left(\widetilde{\mathbf{W}}_{i+1}^{n}+\widetilde{\mathbf{W}}_{i}^{n}\right)-\frac{1}{2}\mathrm{sgn}\left[\widetilde{\mathbf{A}}\left(\overline{\widetilde{\mathbf{W}}}\right)\right]\left(\widetilde{\mathbf{W}}_{i+1}^{n}-\widetilde{\mathbf{W}}_{i}^{n}\right)+\frac{1}{2}\left|\widetilde{\mathbf{A}}\left(\overline{\widetilde{\mathbf{W}}}\right)^{-1}\right|\widetilde{\mathbf{Q}}_{i}^{n}, \tag{3.7a}$$

$$\widetilde{\mathbf{W}}_{i}^{n+1}=\widetilde{\mathbf{W}}_{i}^{n}-\frac{\Delta t}{\Delta x}\left(\widetilde{\mathbf{F}}\left(\widetilde{\mathbf{W}}_{i+\frac{1}{2}}^{n}\right)-\widetilde{\mathbf{F}}\left(\widetilde{\mathbf{W}}_{i-\frac{1}{2}}^{n}\right)\right)+\Delta t\widetilde{\mathbf{Q}}_{i}^{n}, \tag{3.7b}$$

where the averaged state is calculated as

$$\overline{\widetilde{\mathbf{W}}}=\begin{pmatrix}\frac{h_i+h_{i+1}}{2}\\ \frac{h_i+h_{i+1}}{2}\,\frac{u_i\sqrt{h_i}+u_{i+1}\sqrt{h_{i+1}}}{\sqrt{h_i}+\sqrt{h_{i+1}}}\\ \frac{B_i+B_{i+1}}{2}\end{pmatrix}, \tag{3.8}$$

and the sign and inverse matrices are given by

$$\mathrm{sgn}\left[\widetilde{\mathbf{A}}\left(\overline{\widetilde{\mathbf{W}}}\right)\right]=\mathcal{R}\left(\overline{\widetilde{\mathbf{W}}}\right)\mathrm{sgn}\left[\Lambda\left(\overline{\widetilde{\mathbf{W}}}\right)\right]\mathcal{R}^{-1}\left(\overline{\widetilde{\mathbf{W}}}\right),$$
$$\left|\widetilde{\mathbf{A}}\left(\overline{\widetilde{\mathbf{W}}}\right)^{-1}\right|=\mathcal{R}\left(\overline{\widetilde{\mathbf{W}}}\right)\left|\Lambda\left(\overline{\widetilde{\mathbf{W}}}\right)\right|^{-1}\mathcal{R}^{-1}\left(\overline{\widetilde{\mathbf{W}}}\right),$$

with

$$\mathrm{sgn}\left[\Lambda\left(\overline{\widetilde{\mathbf{W}}}\right)\right]=\begin{pmatrix}\mathrm{sgn}\left(\overline{\widetilde{\lambda}}_1\right) & 0 & 0\\ 0 & \mathrm{sgn}\left(\overline{\widetilde{\lambda}}_2\right) & 0\\ 0 & 0 & \mathrm{sgn}\left(\overline{\widetilde{\lambda}}_3\right)\end{pmatrix},$$

and

$$\left|\Lambda\left(\overline{\widetilde{\mathbf{W}}}\right)\right|^{-1}=\begin{pmatrix}\left|\overline{\widetilde{\lambda}}_1\right|^{-1} & 0 & 0\\ 0 & \left|\overline{\widetilde{\lambda}}_2\right|^{-1} & 0\\ 0 & 0 & \left|\overline{\widetilde{\lambda}}_3\right|^{-1}\end{pmatrix},$$

where $\overline{\widetilde{\lambda}}_k$ are the eigenvalues in (2.8) calculated at the averaged solutions. The right and left eigenvector matrices are given by

$$\mathcal{R}\left(\overline{\widetilde{\mathbf{W}}}\right)=\begin{pmatrix}1 & 1 & 1\\ \overline{\widetilde{\lambda}}_1 & \overline{\widetilde{\lambda}}_2 & \overline{\widetilde{\lambda}}_3\\ \frac{-\overline{c}^2-g\overline{B}+\overline{\widetilde{\alpha}}_1^2}{\overline{c}^2} & \frac{-\overline{c}^2-g\overline{B}+\overline{\widetilde{\alpha}}_2^2}{\overline{c}^2} & \frac{-\overline{c}^2-g\overline{B}+\overline{\widetilde{\alpha}}_3^2}{\overline{c}^2}\end{pmatrix}, \tag{3.9a}$$

$$\mathcal{R}^{-1}\left(\overline{\widetilde{\mathbf{W}}}\right)=\begin{pmatrix}\frac{\overline{c}^2+g\overline{B}+\overline{\widetilde{\lambda}}_2\overline{\widetilde{\lambda}}_3-\overline{u}^2}{\overline{\widetilde{\lambda}}_{12}\overline{\widetilde{\lambda}}_{13}} & -\frac{\overline{\widetilde{\alpha}}_2+\overline{\widetilde{\alpha}}_3}{\overline{\widetilde{\lambda}}_{12}\overline{\widetilde{\lambda}}_{13}} & \frac{\overline{c}^2}{\overline{\widetilde{\lambda}}_{12}\overline{\widetilde{\lambda}}_{13}}\\ \frac{\overline{c}^2+g\overline{B}+\overline{\widetilde{\lambda}}_1\overline{\widetilde{\lambda}}_3-\overline{u}^2}{\overline{\widetilde{\lambda}}_{21}\overline{\widetilde{\lambda}}_{23}} & -\frac{\overline{\widetilde{\alpha}}_1+\overline{\widetilde{\alpha}}_3}{\overline{\widetilde{\lambda}}_{21}\overline{\widetilde{\lambda}}_{23}} & \frac{\overline{c}^2}{\overline{\widetilde{\lambda}}_{21}\overline{\widetilde{\lambda}}_{23}}\\ \frac{\overline{c}^2+g\overline{B}+\overline{\widetilde{\lambda}}_1\overline{\widetilde{\lambda}}_2-\overline{u}^2}{\overline{\widetilde{\lambda}}_{31}\overline{\widetilde{\lambda}}_{32}} & -\frac{\overline{\widetilde{\alpha}}_1+\overline{\widetilde{\alpha}}_2}{\overline{\widetilde{\lambda}}_{31}\overline{\widetilde{\lambda}}_{32}} & \frac{\overline{c}^2}{\overline{\widetilde{\lambda}}_{31}\overline{\widetilde{\lambda}}_{32}}\end{pmatrix}, \tag{3.9b}$$

where $\overline{c} = \sqrt{g\overline{h}}$ is the wave speed and

$$\overline{\overline{\alpha}}_k = \overline{\overline{\lambda}}_k - \overline{u}, \quad \overline{\overline{\lambda}}_{kj} = \overline{\overline{\lambda}}_k - \overline{\overline{\lambda}}_j, \quad k,j = 1,2,3.$$

3.2 Approach B

In this approach, the physical variables $\mathbf{U}_{i+1/2}^n$ are used to compute the averaged states in the predictor stage, while the conservative variables $\widetilde{\mathbf{W}}_i^{n+1}$ are updated in the corrector stage. This results in the following scheme for the morphodynamic system (2.6):

$$\mathbf{U}_{i+\frac{1}{2}}^n = \frac{1}{2}\left(\mathbf{U}_{i+1}^n + \mathbf{U}_i^n\right) - \frac{1}{2}\mathrm{sgn}\left[\mathbf{B}\left(\overline{\mathbf{U}}\right)\right]\left(\mathbf{U}_{i+1}^n - \mathbf{U}_i^n\right), \tag{3.10a}$$

$$\widetilde{\mathbf{W}}_i^{n+1} = \widetilde{\mathbf{W}}_i^n - \frac{\Delta t}{\Delta x}\left(\widetilde{\mathbf{F}}\left(\widetilde{\mathbf{W}}_{i+\frac{1}{2}}^n\right) - \widetilde{\mathbf{F}}\left(\widetilde{\mathbf{W}}_{i-\frac{1}{2}}^n\right)\right) + \Delta t\widetilde{\mathbf{Q}}_i^n, \tag{3.10b}$$

where the averaged state is calculated as

$$\overline{\mathbf{U}} = \begin{pmatrix} \frac{h_i+h_{i+1}}{2} \\ \frac{u_i\sqrt{h_i}+u_{i+1}\sqrt{h_{i+1}}}{\sqrt{h_i}+\sqrt{h_{i+1}}} \\ \frac{B_i+B_{i+1}}{2} \end{pmatrix}, \tag{3.11}$$

and the sign matrix is given by

$$\mathrm{sgn}\left[\mathbf{B}\left(\overline{\mathbf{U}}\right)\right] = \mathcal{R}\left(\overline{\mathbf{U}}\right)\mathrm{sgn}\left[\Lambda\left(\overline{\mathbf{U}}\right)\right]\mathcal{R}^{-1}\left(\overline{\mathbf{U}}\right), \tag{3.12}$$

with

$$\mathrm{sgn}\left[\Lambda\left(\overline{\mathbf{U}}\right)\right] = \begin{pmatrix} \mathrm{sgn}\left(\overline{\mu}_1\right) & 0 & 0 \\ 0 & \mathrm{sgn}\left(\overline{\mu}_2\right) & 0 \\ 0 & 0 & \mathrm{sgn}\left(\overline{\mu}_3\right) \end{pmatrix}, \tag{3.13}$$

where $\overline{\mu}_k$ are the eigenvalues in (2.11) calculated at the averaged solutions. The right and left eigenvector matrices are given by

$$\mathcal{R}\left(\overline{\mathbf{U}}\right) = \begin{pmatrix} 1 & 1 & 1 \\ \frac{\overline{\beta}_1}{\overline{h}} & \frac{\overline{\beta}_2}{\overline{h}} & \frac{\overline{\beta}_3}{\overline{h}} \\ \frac{\overline{\beta}_1^2-\overline{c}^2}{\overline{c}^2} & \frac{\overline{\beta}_2^2-\overline{c}^2}{\overline{c}^2} & \frac{\overline{\beta}_3^2-\overline{c}^2}{\overline{c}^2} \end{pmatrix}, \tag{3.14a}$$

$$\mathcal{R}^{-1}\left(\overline{\mathbf{U}}\right) = \begin{pmatrix} \frac{\overline{c}^2+\overline{\beta}_2\overline{\beta}_3}{\overline{\mu}_{12}\overline{\mu}_{13}} & -\frac{h(\overline{\beta}_2+\overline{\beta}_3)}{\overline{\mu}_{12}\overline{\mu}_{13}} & \frac{\overline{c}^2}{\overline{\mu}_{12}\overline{\mu}_{13}} \\ \frac{\overline{c}^2+\overline{\beta}_1\overline{\beta}_3}{\overline{\mu}_{21}\overline{\mu}_{23}} & -\frac{h(\overline{\beta}_1+\overline{\beta}_3)}{\overline{\mu}_{21}\overline{\mu}_{23}} & \frac{\overline{c}^2}{\overline{\mu}_{21}\overline{\mu}_{23}} \\ \frac{\overline{c}^2+\overline{\beta}_1\overline{\beta}_2}{\overline{\mu}_{31}\overline{\mu}_{32}} & -\frac{h(\overline{\beta}_1+\overline{\beta}_2)}{\overline{\mu}_{31}\overline{\mu}_{32}} & \frac{\overline{c}^2}{\overline{\mu}_{31}\overline{\mu}_{32}} \end{pmatrix}, \tag{3.14b}$$

where $\bar{c} = \sqrt{gh}$ is the wave speed and

$$\overline{\beta}_k = \overline{\mu}_k - \overline{u}, \qquad \overline{\mu}_{kj} = \overline{\mu}_k - \overline{\mu}_j, \qquad k, j = 1, 2, 3.$$

Remark that, since the predictor stage in (3.10a) and (3.10b) uses the physical variables $\mathbf{U}^n_{i+1/2}$, the source term appears only in the corrector stage.

3.3 Approach C

In this approach, the physical variables are used in both the predictor and corrector stages. This results in the following scheme for the morphodynamic system (2.9)

$$\mathbf{U}^n_{i+\frac{1}{2}} = \frac{1}{2}\big(\mathbf{U}^n_{i+1} + \mathbf{U}^n_i\big) - \frac{1}{2}\mathrm{sgn}\big[\mathbf{B}\big(\overline{\mathbf{U}}\big)\big]\big(\mathbf{U}^n_{i+1} - \mathbf{U}^n_i\big), \tag{3.15a}$$

$$\mathbf{U}^{n+1}_i = \mathbf{U}^n_i - \frac{\Delta t}{\Delta x}\big(\mathbf{G}\big(\mathbf{U}^n_{i+\frac{1}{2}}\big) - \mathbf{G}\big(\mathbf{U}^n_{i-\frac{1}{2}}\big)\big), \tag{3.15b}$$

where the averaged sate $\overline{\mathbf{U}}$ is given in (3.11) and the sign matrix $\mathrm{sgn}[\mathbf{B}(\overline{\mathbf{U}})]$ is given by (3.12)-(3.14b). Note that no source treatment is required in the predictor-corrector procedure (3.15).

4 Approximation of the source terms

The treatment of source terms in shallow water equations is crucial for the performance of most finite volume methods. In the proposed finite volume methods, the discretization of the source terms is carried out such that it is well balanced with discretization of the flux gradients using the concept of C-property [4]. Recall that, a numerical scheme is said to satisfy the C-property for a morphodynamic problem if the condition

$$B^n = \bar{B}(x), \qquad h^n + B^n = C, \qquad u^n = 0, \tag{4.1}$$

holds for stationary flows. Here, $\bar{B}(x)$ is a fixed bed and C is a constant. Therefore, the treatment of source terms in the above approaches is reconstructed such that the condition (4.1) is preserved at the discretized level. It should be pointed out that this property is fundamental for the correct transport of bed-load by water flows. A numerical scheme which does not satisfy the C-property may produce nonphysical oscillations in the bed resulting in poor resolution of shocks and instability problems.

For brevity in presentation we describe the approximation of the source terms only for the Approach A. For the Approach B a similar procedure applied. Let us assume a stationary flow at rest, $u = 0$. Thus, the Exner equation (2.2) yields that the bed B is constant in time, i.e., $B(t, x) = \bar{B}(x)$, and the morphodynamic system (2.6) reduces to

$$\partial_t \begin{pmatrix} h \\ 0 \end{pmatrix} + \partial_x \begin{pmatrix} 0 \\ \frac{1}{2}gh^2 \end{pmatrix} = \begin{pmatrix} 0 \\ -gh\partial_x B \end{pmatrix}. \tag{4.2}$$

The matrices $\mathbf{R}$, $\mathbf{\Lambda}$ and $\mathbf{R}^{-1}$ appeared in (3.7) for the approach A are defined as

$$\mathbf{R}^n_{i+\frac{1}{2}} = \begin{pmatrix} 1 & 1 \\ -c & c \end{pmatrix}, \quad \mathbf{\Lambda}^n_{i+\frac{1}{2}} = \begin{pmatrix} -c & 0 \\ 0 & c \end{pmatrix}, \quad \left(\mathbf{R}^n_{i+\frac{1}{2}}\right)^{-1} = \frac{1}{2}\begin{pmatrix} 1 & -c^{-1} \\ 1 & c^{-1} \end{pmatrix},$$

where

$$c = \sqrt{g\frac{h^n_i + h^n_{i+1}}{2}},$$

is the wave speed calculated at the interface $x_{i+1/2}$ of the control volume. Applied to the system (4.2), the predictor stage in (3.7) computes

$$\widetilde{\mathbf{W}}^n_{i+\frac{1}{2}} = \begin{pmatrix} \frac{h^n_i + h^n_{i+1}}{2} \\ \frac{1}{2}c^n_{i+\frac{1}{2}}\left(h^n_{i+1} + B^n_{i+1} - h^n_i - B^n_i\right) \end{pmatrix}, \tag{4.3}$$

while the corrector stage in (3.10a) and (3.10b) updates the solution as

$$\widetilde{\mathbf{W}}^{n+1}_i = \widetilde{\mathbf{W}}^n_i - g\frac{\Delta t}{2\Delta x}\begin{pmatrix} 0 \\ \left(h^n_{i+\frac{1}{2}}\right)^2 - \left(h^n_{i-\frac{1}{2}}\right)^2 \end{pmatrix} - \Delta t \begin{pmatrix} 0 \\ \left(gh\partial_x B\right)^n_i \end{pmatrix}. \tag{4.4}$$

To obtain a stationary solution $\widetilde{\mathbf{W}}^{n+1}_i = \widetilde{\mathbf{W}}^n_i$, the sum of discretized flux gradients and source terms in (4.4) should be equal to zero, i.e.,

$$g\frac{1}{2\Delta x}\left(\left(h^n_{i+\frac{1}{2}}\right)^2 - \left(h^n_{i-\frac{1}{2}}\right)^2\right) = -\left(gh\partial_x B\right)^n_i. \tag{4.5}$$

Using

$$h^n_{i+\frac{1}{2}} = \frac{h^n_i + h^n_{i+1}}{2},$$

the condition (4.5) is equivalent to

$$g\frac{1}{8\Delta x}\left(h^n_{i+1} + 2h^n_i + h^n_{i-1}\right)\left(h^n_{i+1} - h^n_{i-1}\right) = -\left(gh\partial_x B\right)^n_i. \tag{4.6}$$

Since for stationary solution

$$h^n_{i+1} - h^n_{i-1} = B^n_{i+1} - B^n_{i-1},$$

the Eq. (4.6) becomes

$$\left(gh\partial_x B\right)^n_i = g\frac{h^n_{i+\frac{1}{2}} + h^n_{i-\frac{1}{2}}}{2}\frac{B^n_{i+1} - B^n_{i-1}}{2\Delta x}. \tag{4.7}$$

Hence, if the source term in the corrector stage of (3.7) is discretized as

$$\mathbf{Q}^n_i = \begin{pmatrix} 0 \\ g\frac{h^n_{i+\frac{1}{2}} + h^n_{i-\frac{1}{2}}}{2}\frac{B^n_{i+1} - B^n_{i-1}}{2\Delta x} \\ 0 \end{pmatrix}, \tag{4.8}$$

then the proposed finite volume method satisfies the C-property.

5 Extension to the second-order accuracy

Obviously, the proposed finite volume method is only first-order accurate in both space and time. To extend its accuracy to a second-order scheme, we use a MUSCL method incorporating slope limiters in the spatial discretization and a two-step Runge-Kutta method for time integration. The MUSCL discretization uses an approximation of the solution state W by a linear interpolation at each cell interface, see for example [11]. In the present work, we consider a second-order scheme incorporating limiters in its reconstruction. Thus, the numerical flux (3.3) becomes

$$W^n_{i+\frac{1}{2}} = \frac{1}{2}\big(W^{n-}_{i+\frac{1}{2}} + W^{n+}_{i+\frac{1}{2}}\big) - \frac{1}{\Delta x}\theta^n_{i+\frac{1}{2}}\big(F(W^{n+}_{i+\frac{1}{2}}) - F(W^{n-}_{i+\frac{1}{2}})\big) + \theta^n_{i+\frac{1}{2}} Q^n_{i+\frac{1}{2}}, \tag{5.1}$$

where the states states $W^{n+}_{i+1/2}$ and $W^{n-}_{i+1/2}$ are defined as

$$W^{n-}_{i+\frac{1}{2}} = W^n_i + \frac{1}{2}\Phi(r_i)(W^n_{i+1} - W^n_i), \tag{5.2a}$$

$$W^{n+}_{i+\frac{1}{2}} = W^n_{i+1} - \frac{1}{2}\Phi(r_{i+1})(W^n_{i+2} - W^n_{i+1}), \tag{5.2b}$$

with the slope r_i is given by

$$r_i = \frac{W^n_i - W^n_{i-1}}{W^n_{i+1} - W^n_i}.$$

Note that, for the morphodynamic system (2.4), the second-order reconstruction (5.1) has to be performed for the physical variables h, u and B. In (5.2), $\Phi(r)$ defines the slope limiter function such as the Minmod function

$$\Phi(r) = \max\big\{0, \min\{1, r\}\big\}, \tag{5.3}$$

or the van leer function

$$\Phi(r) = \frac{|r| + r}{1 + |r|}. \tag{5.4}$$

Remark that other slope limiter functions from [11] can also apply. Remark that if we set $\Phi = 0$, the spatial discretization (5.1) reduces to the first-order scheme.

6 Numerical results and examples

Three test examples are selected to check the accuracy and the performance of the proposed finite volume schemes. As with all explicit time stepping methods the theoretical maximum stable time step Δt is specified according to the Courant-Friedrichs-Lewy (CFL) condition

$$\Delta t = Cr\frac{\Delta x}{\max\limits_{k=1,2,3}\big(|\lambda^n_k|\big)}, \tag{6.1}$$

where Cr is a constant to be chosen less than unity. In all our simulations, the fixed Courant number $Cr = 0.8$ is used and the time step is varied according to (6.1). For the considered test examples, the channel is of length 1000m and the initial water level and initial velocity are given as

$$h(0,x) = 10\text{m} - B(0,x) \quad \text{and} \quad u(0,x) = \frac{10\text{m}/\text{s}^2}{h(0,x)}.$$

Furthermore, the porosity constant $p = 0.4$ and two values $A = 0.001$ and $A = 1$ are used in the sediment transport flux (2.3). Note that, large or small values of A characterize respectively, a fast or slow interaction between the bed-load and the water flow in the morphodynamical problem. It is worth remarking that, for the considered value of the discharge $Q = 10\text{m}^2/\text{s}$, the Froude number $Fr = u/\sqrt{gh} \approx 0.1$. To obtain realistic initial data for the morphodynamic equations, we first solve the shallow water equations (2.1) keeping the channel bed fixed until an equilibrium state is reached. The computed solutions h and u are then used for moving bed simulations. In all our computations, unless stated, the spatial stepsize $\Delta x = 10\text{m}$ and the Van leer limiter function is used.

6.1 Example 1

We consider the test example of the evolution of an initially hump-shaped bed in a channel studied in [9]. The initial bed is defined as

$$B(0,x) = \begin{cases} \sin^2\left(\frac{(x-300)\pi}{200}\right), & \text{if } 300 \leq x \leq 500, \\ 0, & \text{elsewhere.} \end{cases}$$

In Fig. 2 we present the initial bed-load along with the initial water height. In the first run for this test example we set $A = 0.001$ resulting in a slow interaction between the

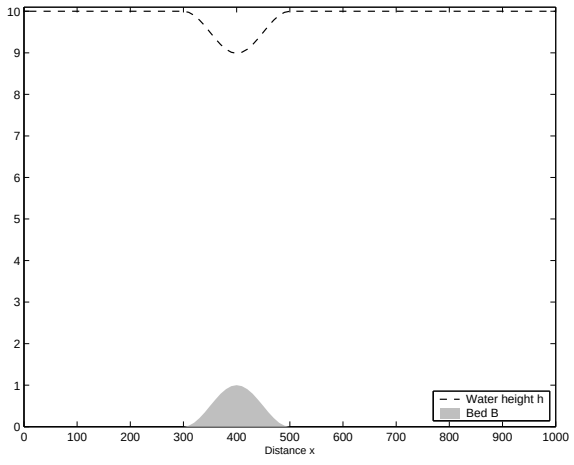

Figure 2: Initial bed-load and water height for Example 1.

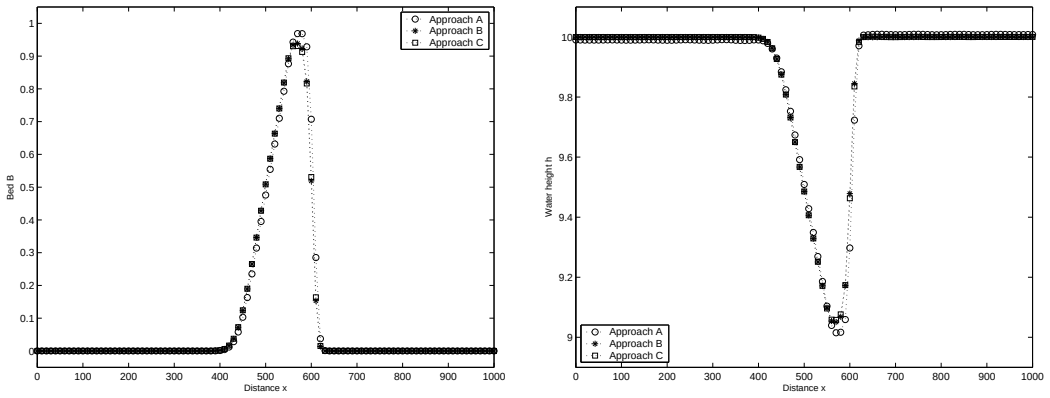

(a) (b)

Figure 3: Bed-load (a) and water height (b) for Example 1 with $A = 0.001$ at $t = 238000$s.

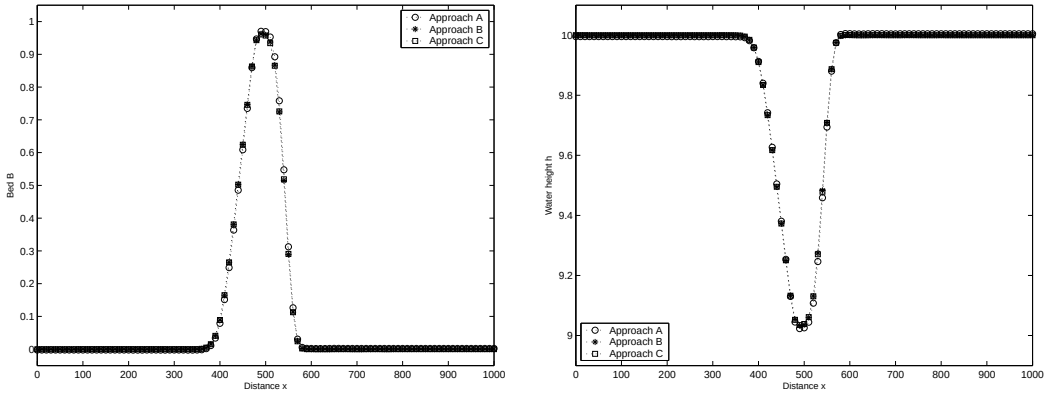

(a) (b)

Figure 4: Bed-load (a) and water height (b) for Example 1 with $A = 1$ at $t = 238$s.

bed-load and the water flow. In Fig. 3 we display the bed profiles and water height at time $t = 238000$s computed using the three approaches. In all considered approaches, the upper front of the hump travels faster than the lower base so that the propagating bed-load creates a shock at the front after a certain time. The obtained results demonstrate the ability of the presented finite volume scheme to capture traveling fronts without generating spurious oscillations. It is evident that the results obtained using Approach B and Approach C are more diffusive than those obtained using Approach A. Next, results obtained for $A = 1$ at $t = 238$s are displayed in Fig. 4. In this later case, no pronounced differences are detected between the results obtained using the three approaches. The finite volume scheme performs well for this sediment transport problem since it does not diffuse the moving bed and no spurious oscillations have been observed when the water flows over the bed profile. Furthermore, the obtained results compare favorably with those reported in [9] for the same sediment transport problem.

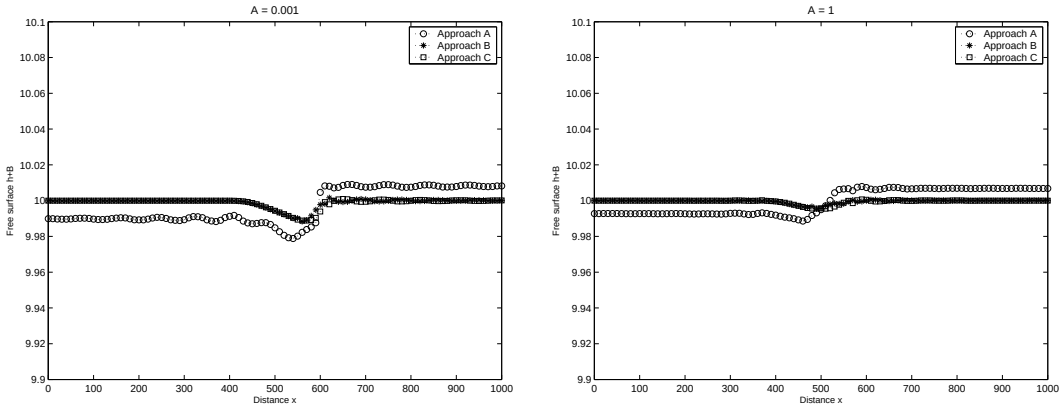

(a) (b)

Figure 5: Free surface for Example 1 with $A = 0.001$ at $t = 238000$s (a) and with $A = 1$ at $t = 238$s (b).

To examine the performance of the proposed approaches in preserving the C-property we present in Fig. 5 the free surface with $A = 0.001$ at time $t = 238000$s and with $A = 1$ at time $t = 238$s. It can be noted the perturbations occurring in the computational domain are slightly different for all approaches and extend to regions far from the bed-load. This can be interpreted by the fact that the velocity field is not entirely uniform across the channel with high-amplitude velocities occurring in the center. These variations in the velocity field across the channel produce variations in

Table 1: Relative errors for Example 1 with $A = 0.001$ at $t = 5000$s.

			Approach A			
N	L^1-error	Rate	L^∞-error	Rate	L^2-error	Rate
50	4.90240E-05	—	3.53989E-04	—	9.84635E-05	—
100	2.50423E-05	0.97	1.92992E-04	0.88	5.66608E-05	0.80
200	1.21406E-05	1.04	9.48070E-05	1.03	2.95266E-05	0.94
400	6.00069E-06	1.02	4.76398E-05	1.00	1.49603E-05	0.98
800	3.00783E-06	1.00	2.40495E-05	0.99	7.49793E-06	1.00
			Approach B			
N	L^1-error	Rate	L^∞-error	Rate	L^2-error	Rate
50	5.58887E-05	—	3.87988E-04	—	1.18881E-04	—
100	2.57356E-05	1.12	1.93998E-04	1.00	6.00037E-05	0.99
200	1.23546E-05	1.06	9.59990E-05	1.01	3.01062E-05	0.99
400	6.05556E-06	1.03	4.81047E-05	1.00	1.50481E-05	1.00
800	3.02656E-06	1.00	2.43552E-05	0.98	7.53506E-06	1.00
			Approach C			
N	L^1-error	Rate	L^∞-error	Rate	L^2-error	Rate
50	1.10740E-03	—	1.32646E-03	—	1.12601E-03	—
100	5.88571E-04	0.91	7.05562E-04	0.91	5.98523E-04	0.91
200	2.79634E-04	1.07	4.05870E-04	0.80	2.84973E-04	1.07
400	1.21627E-04	1.20	2.55959E-04	0.67	1.24256E-04	1.20
800	3.95572E-05	1.62	1.75985E-04	0.54	4.09563E-05	1.60

the morphology of the bed given the fact that the sediment transport flux is a function of u^3. We also note that the velocity field evolves along with the morphological changes.

Our next concern is to perform a convergence study for the proposed finite volume method for this test example. This problem cannot be solved analytically and therefore a numerical solution, computed on a fine mesh of 1600 gridpoints, is adopted as the reference solution. The relative L^1, L^∞ and L^2 errors are listed in Table 1 for $A = 0.001$ at $t = 5000$s using different numbers of gridpoints N. All the errors are measured by the difference between the pointvalues of the reference solution and the reconstructed pointvalues of the computed solution. For sake of comparison, we have also included the convergence rates in Table 1. It is clear that increasing the number of gridpoinds in the space domain results in a decrease of all error-norms for all approaches. In terms of all considered error-norms, the Approach A could be the most accurate among the other approaches for solving morphodynamic problems. A slower decrease in these error-norms has been observed in Approach C than those obtained using Approach B and Approach A. This behavior in Approach C may be attributed to the use of the non-conservative form of the sediment transport problem resulting in an absence of any numerical treatment of the source term in (3.15). It is worth remarking that for large values of A, faster decay on the errors has been detected in the considered approaches.

6.2 Example 2

This test problem considers the evolution of an initially discontinuous bed in a channel proposed in [6]. Due to this discontinuity in the initial bed profile, this test example is more challenging than the previous example. The initial bed is defined as

$$B(0,x) = \begin{cases} 1, & \text{if } 300 \leq x \leq 500, \\ 0, & \text{elsewhere.} \end{cases}$$

This initial bed-load and the initial water height are presented in Fig. 6. The evolution of the bed profile and the water height with $A = 0.001$ at time $t = 580000$s is depicted

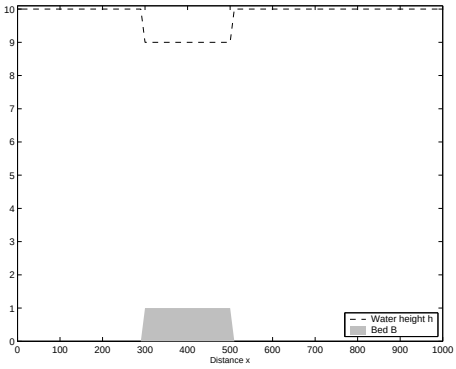

Figure 6: Initial bed-load and water height for Example 2.

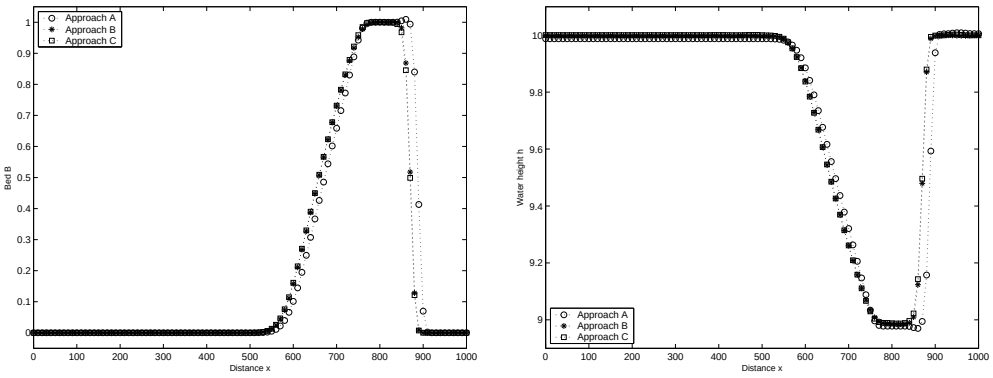

(a) (b)

Figure 7: Bed-load (a) and water height (b) for Example 2 with $A = 0.001$ at $t = 580000$s.

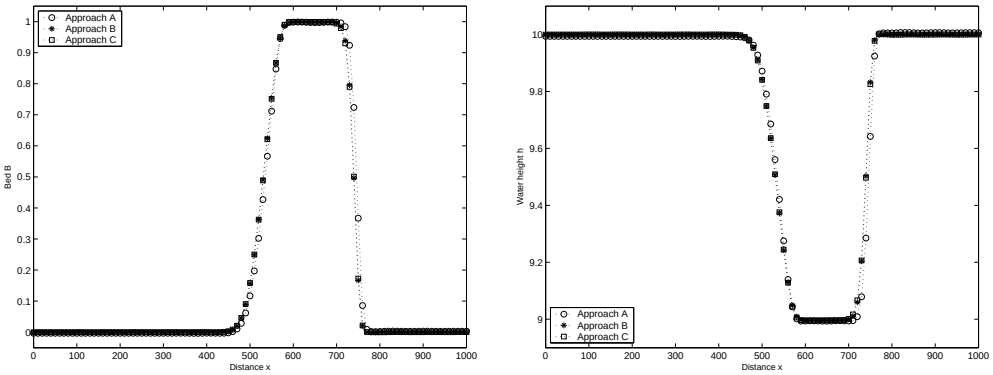

(a) (b)

Figure 8: Bed-load (a) and water height (b) for Example 2 with $A = 1$ at $t = 624$s.

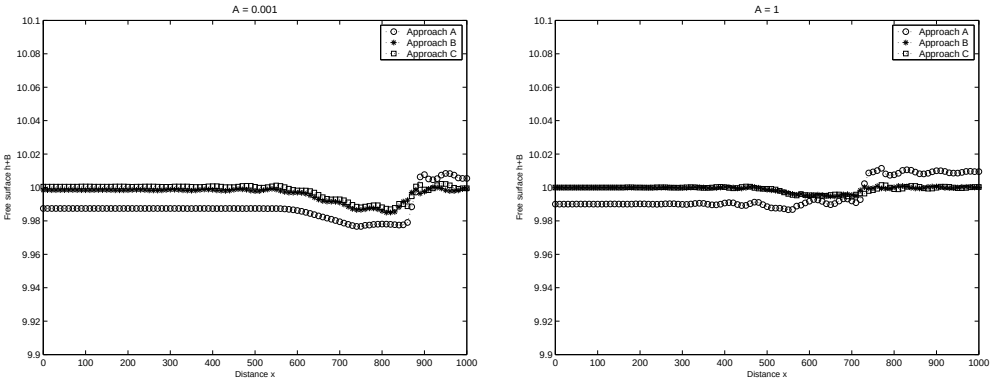

(a) (b)

Figure 9: Free surface for Example 2 with $A = 0.001$ at $t = 580000$s (a) and with $A = 1$ at $t = 624$s (b).

in Fig. 7. The results with $A = 1$ at time $t = 624$s are included in Fig. 8 for the three approaches. The computed water free surfaces are plotted in Fig. 9 for both test cases.

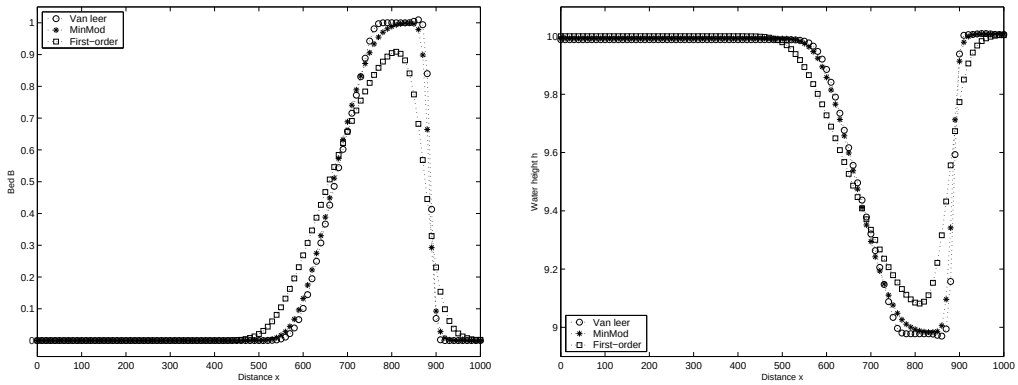

(a) (b)

Figure 10: Comparison between results obtained using different limiters for bed-load (a) and water height (b) for Example 2 with $A = 0.001$ at $t = 580000$s.

Again the proposed finite volume scheme performs accurately for this test example. It is clear that the results computed using Approach B and Approach C are roughly the same, whereas the results obtained using Approach A are slightly more accurate. The proposed finite volume method performs very satisfactorily for this nonlinear coupled problem since it does not diffuse the moving bed fronts and no spurious oscillations have been detected near steep gradients of the flow field in the computational domain.

We now turn our attention to examine the limiters used for the second-order reconstruction (5.1). To this end we illustrate in Fig. 10 the bed profile and the water height with $A = 0.001$ at time $t = 580000$s obtained using the Minmod and Van leer limiter functions. The first-order results are also included in this figure. The high accuracy of the second-order finite volume over its first-order counterpart is clearly demonstrated in both, bed-load and water height variables. Similar behavior has been detected for the other test examples. In all our simulations, the results obtained using the Minmod limiter are more diffusive than those obtained using the Van leer limiter.

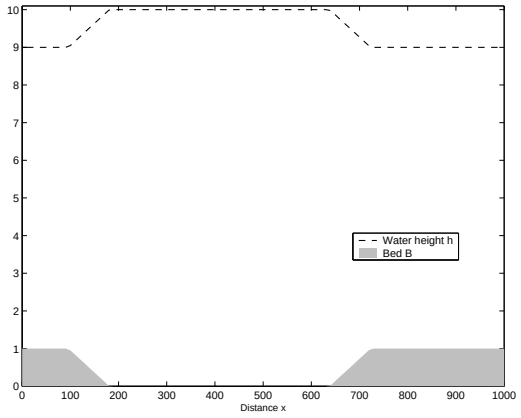

Figure 11: Initial bed-load and water height for Example 3.

6.3 Example 3

Our final test example is the problem of a sediment transport with backward/forward step. Here the initial bed is defined as

$$B(0,x) = \begin{cases} 1, & \text{if } 0 \leq x \leq 96, \\ \frac{-x+181}{85}, & \text{if } 96 \leq x \leq 181, \\ 0, & \text{if } 181 \leq x \leq 638, \\ \frac{x-638}{85}, & \text{if } 638 \leq x \leq 723, \\ 1, & \text{if } 723 \leq x \leq 1000. \end{cases}$$

A similar test example was studied in [7] for sedimentary flows. Fig. 11 illustrates the initial bed-load and the initial water height. We display in Fig. 12 the bed-load and the water height with $A = 0.001$ at time $t = 250000$s. Fig. 13 reports the obtained

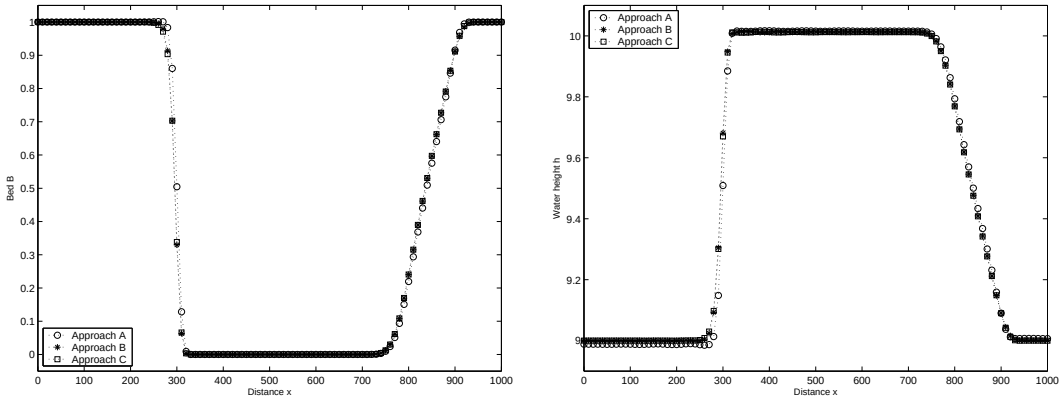

(a) (b)

Figure 12: Bed-load (a) and water height (b) for Example 3 with $A = 0.001$ at $t = 250000$s.

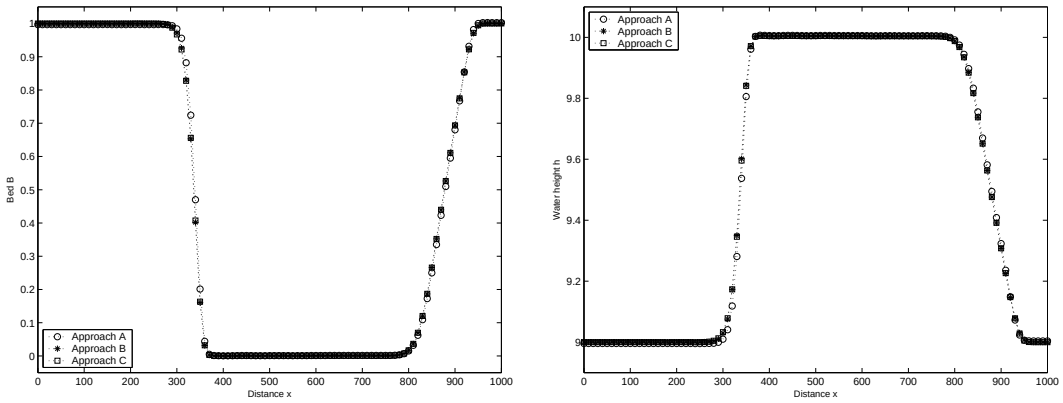

(a) (b)

Figure 13: Bed-load (a) and water height (b) for Example 3 with $A = 1$ at $t = 482$s.

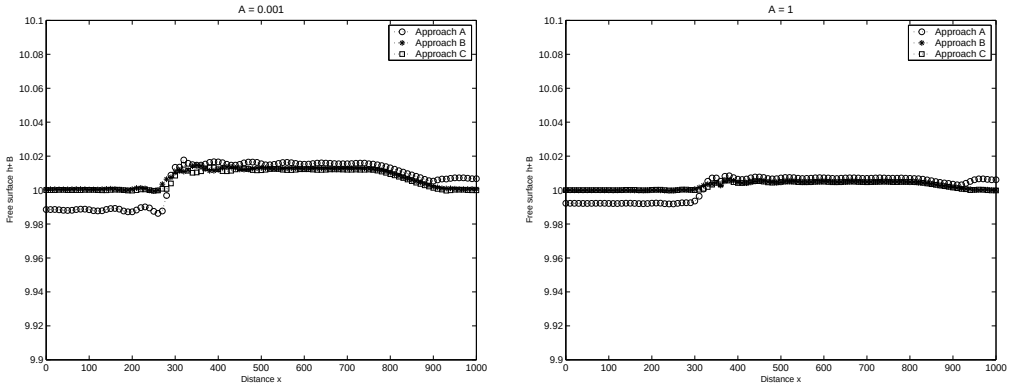

(a) (b)

Figure 14: Free surface for Example 3 with $A = 0.001$ at $t = 250000$s (a) and with $A = 1$ at $t = 482$s (b).

results with $A = 1$ at $t = 482$s. The free surface with $A = 0.001$ at time $t = 250000$s and with $A = 1$ at time $t = 482$s are shown in Fig. 14. As in the previous test examples, all the considered approaches exhibit similar structures for both water flow and bed profile. Note that the performance of the proposed finite volume method is very attractive since the computed solutions remain stable and oscillation-free even for relatively coarse grids without solving nonlinear systems or Riemann problems.

Finally, analysis of computational cost has been carried out in the considered test examples. Table 2 summarizes the computational cost of the three approaches for the considered test examples with $A = 0.001$. As can be observed, there is little difference between the three approaches applied to the same test example. However, it is clear that the Approach C required less CPU time than Approach A and Approach B. Therefore, bearing in mind the slight change in the results from all approaches at the expense of rather small increase in CPU times, the considered approaches are believed to be adequate to obtain accurate and efficient results for practical morphodynamic problems. It is worth mentioning that the CPU times in the considered approaches can be drastically reduced by considering implicit time integration scheme along with multigrid techniques to speed up the convergence in the solution of linear systems, see [12] among others. This type of methods can be executed with time steps much more larger than for the explicit methods. This fact allows much fewer time steps to be taken for the same period of simulation, thereby reducing the total computational cost tremendously.

Table 2: CPU times (in minutes) for the simulations with $A = 0.001$ for the three examples.

	Example 1 $t = 238000$s	Example 2 $t = 580000$s	Example 3 $t = 250000$s
Approach A	8.27	20.03	9.56
Approach B	7.38	18.05	7.93
Approach C	6.90	16.83	7.17

7 Conclusions

In this paper we have studied the accuracy and efficiency of a class of finite volume methods for numerical solution of morphodynamic problems in coastal regions. The proposed finite volume method consists of two stages which can be viewed as a predictor-corrector procedure. In the first stage, the scheme reconstructs the numerical fluxes using the sign matrix of the flux Jacobian in the morphodynamic equations. This stage results in an upwind discretization of the characteristic variables and avoids the singularity that may occur in the Jacobian matrix for the conservative form of the morphodynamic equations. In the second stage, the solution is updated using a special treatment of the bed bottom in order to obtain a well-balanced discretization of the flux gradient and the source term. Three approaches have been discussed depending on the form of morphodynamic equations used in the predictor procedure. To increase the accuracy of the finite volume methods we have incorporated slope limiters.

The methods have been numerically examined for several test examples in morphodynamic problems with different initial beds in a channel. We have compared the numerical results obtained for three finite volume approaches. In most cases, the proposed methods have exhibited accurate prediction of both, the free surface and the bed-load with correct C-property, and stable representation of free surface response to the movable bed. The results make it promising to be applicable also to real situations where, beyond the many sources of complexity, there is a more severe demand for accuracy in predicting the morphological evolution, which must be performed for long time. Future work will concentrate on developing efficient time integration schemes for the finite volume discretization and extension of these approaches to morphodynamic flow problems in two space dimensions.

Acknowledgments

This work was partly performed while the third author was a visiting professor at CMLA, École normale supérieure de Cachan. Financial support provided by CLMA, ENS Cachan is gratefully acknowledged.

References

[1] F. Benkhaldoun, I. Elmahi and M. Seaïd, *Well-balanced finite volume schemes for pollutant transport by shallow water equations on unstructured meshes*, J. Comput. Phys., 226 (2007), pp. 180–203.

[2] F. Benkhaldoun, S. Sahmim and M. Seaïd, *A two-dimensional finite volume morphodynamic model on unstructured triangular grids*, Int. J. Numer. Meth. Fluids., 63 (2001), pp. 1296–1327.

[3] F. Benkhaldoun, S. Sahmim and M. Seaïd, *Solution of the sediment transport equations using a finite volume method based on sign matrix*, SIAM J. Sci. Comput., 31 (2009), pp. 2866–2889.

[4] A. BERMÚDEZ AND E. M. VÁZQUEZ, *Upwind methods for hyperbolic conservation laws with source terms*, Comput. Fluids., 23 (1994), pp. 1049–1071.
[5] V. CALEFFI, A. VALIANI AND A. BERNINI, *High-order balanced CWENO scheme for movable bed shallow water equations*, Adv. Water. Res., 30 (2007), pp. 730–741.
[6] N. Z. CRNJARIC, S. VUKOVIC AND L. SOPTA, *Extension of ENO and WENO schemes to one-dimensional sediment transport equations*, Comput. Fluids., 33 (2004), pp. 31–56.
[7] A. CROTOGINO AND K. P. HOLZ, *Numerical movable-bed models for practical engineering*, Appl. Math. Model., 8 (1984), pp. 45–49.
[8] A. I. DELIS AND I. PAPOGLOU, *Relaxation approximation to bed-load sediment transport*, J. Comput. Appl. Math., 213 (2008), pp. 521–546.
[9] J. HUDSON AND P. K. SWEBY, *Formations for numerically approximating hyperbolic systems governing sediment transport*, J. Sci. Comput., 19 (2003), pp. 225–252.
[10] A. J. GRASS, *Sediment transport by waves and currents*, SERC London Cent. Mar. Technol., Report No: FL29, 1981.
[11] J. L. RANDALL, *Numerical Methods for Conservation Laws*, Lect. Math. ETH Zürich., 1992.
[12] C. LIANG, R. KANNAN AND Z. J. WANG, *A p-multigrid spectral difference method with explicit and implicit smoothers on unstructured triangular grids*, Comput. Fluids., 38 (2009), pp. 254–265.
[13] W. LONG, J. T. KIRBY AND Z. SHAO, *A numerical scheme for morphological bed level calculations*, Coastal. Eng., 55 (2008), pp. 167–180.
[14] J. M. MASELLA, I. FAILLE AND T. GALLOUËT, *On an approximate Godunov scheme*, Int. J. Comput. Fluids. Dyn., 13 (1999), pp. 133–149.
[15] D. PRITCHARD AND A. J. HOGG, *On sediment transport under dam-break flow*, J. Fluid. Mech., 473 (2002), pp. 265–274.
[16] P. L. ROE, *Approximate Riemann solvers, parameter vectors and difference schemes*, J. Comput. Phys., 43 (1981), pp. 357–372.
[17] G. ROSATTI AND L. FRACCAROLLO, *A well-balanced approach for flows over mobile-bed with high sediment-transport*, J. Comput. Phys., 220 (2006), pp. 312–338.
[18] S. SAHMIM, F. BENKHALDOUN AND F. ALCRUDO, *A sign matrix based scheme for quasi-hyperbolic non-homogeneous PDEs with an analysis of the convergence stagnation problem*, J. Comput. Phys., 226 (2007), pp. 1753–1783.
[19] S. SAHMIM, Un Schéma aux Volumes Finis avec Matrice Signe pour les Systémes Non Homogénes, Dissertation, University of Paris 13, 2005.
[20] M. E. VÁZQUEZ, *Improved treatment of source terms in upwind schemes for the shallow water equations in channels with irregular geometry*, J. Comput. Phys., 148 (1999), pp. 497–526.